Available online at www.sciencedirect.com

SciVerse ScienceDirect

Journal of the European Ceramic Society 32 (2012) 1775–1786

www.elsevier.com/locate/jeurceramsoc

A study of the microstructure and mechanical properties of SiC coatings on spherical particles

Huixing Zhang, Eddie López-Honorato [a], Athar Javed, Xiaofeng Zhao, Jun Tan, Ping Xiao *

Materials Science Centre, School of Materials, University of Manchester, M1 7HS, UK

Received 15 June 2011; received in revised form 28 November 2011; accepted 11 December 2011
Available online 30 January 2012

Abstract

We have investigated the effect of the microstructure on the mechanical properties of three nearly stoichiometric SiC coatings (SiC, SiC + C and SiC + Si coating), which were coated onto spherical particles as simulated nuclear fuel particles by fluidized-bed chemical vapour deposition (FBCVD). The mechanical properties of the SiC coatings were studied using micro- and nano-indentation. The microstructure was characterised using scanning electron microscopy (SEM) and transmission electron microscopy (TEM). TEM was also used to elucidate the deformation behaviour under the indentation. The FBCVD SiC coatings studied exhibited a higher hardness than conventional CVD SiC coatings, and SiC coating gave the highest hardness among the three coatings. TEM confirmed that the presence of pores affect the Young's modulus of SiC coatings. The high hardness was attributed to the high density of dislocations and their interactions. The initiation and propagation of micro cracks under the confined shear stress was found to be responsible for the mechanism of plastic deformation. Based on this hardness-related plastic deformation mechanism, the variation of hardness in the three types of SiC coating was due to different grain morphologies.

Keywords: FBCVD SiC coating; Sub-micrometres polycrystalline; Hardness; Young's modulus; Indentation; TEM

1. Introduction

The silicon carbide (SiC) coating in the Tri-isotropic (TRISO) fuel particles is of interest to the nuclear industry due to its small neutron-capture cross-section and strong covalent/ionic Si–C bond,[1] which give long term resistance to irradiation and excellent mechanical properties. The SiC coating is the most important component for structural integrity of TRISO fuel particles as it sustains most of the internal pressure produced by the fission gases produced in the kernel.[2,3] Young's modulus and hardness are mechanical properties used in modeling to estimate the failure probability of TRISO fuel particles.[4] The values at room temperature are used due to that Young's modulus slightly decreased at elevated temperature in SiC material, and the higher value could be kept until temperature reached 2000 °C.[1] It was also found that SiC material with higher hardness at room temperature persist higher hardness value at temperature up to 1600 °C.[1] To achieve a reliable fuel design, a better understanding of the mechanical properties of the SiC layer at room temperature needs to be established. It is difficult to use traditional methods to measure hardness and Young's modulus due to the small dimension of the TRISO fuel particles (∼1 mm). Nano-indentation has made it possible to measure the hardness and Young's modulus accurately[5,6] for a coating of such a small dimension. Furthermore, this method also offers the ability to study the deformation behaviour under the indentation[7–12] as the indentation stress field is of a localized character.

López-Honorato et al.[5] study of SiC deposited at 1300 °C by fluidized bed chemical vapour deposition (FBCVD) showed that the SiC coatings produced under those conditions had high hardness (>42 GPa) and Young's modulus (∼455 GPa). They found that even samples with the composition of SiC + C or SiC + Si showed high mechanical properties. Further, it was shown that the coatings had submicrometer (<1 μm diameter) grain size, but due to the complex microstructure the mechanism controlling the hardness and Young's modulus was unknown. Various groups[10,11,13–16] have made efforts to study the deformation mechanism under

* Corresponding author. Tel.: +44 161 3065941; fax: +44 161 3063586.
E-mail address: Ping.Xiao@manchester.ac.uk (P. Xiao).
[a] Currently at the European Commission, Joint Research Centre, Institute for Transuranium Elements, Germany.

0955-2219/$ – see front matter © 2012 Elsevier Ltd. All rights reserved.
doi:10.1016/j.jeurceramsoc.2011.12.014

indentation in SiC single crystals and polycrystals (with a grain size < 100 nm or grain size > 1 μm). Szlufarska et al.[15] suggested a crossover mechanism from indentation-induced crystallization to deformation-dominated amorphization in nano-crystalline SiC. From the work reported[11,16,17] it is clear that dislocation initiation and propagation is the primary response for the plastic deformation under an indentation in single crystal and polycrystalline (>1 μm) SiC. Further, it has also been found while studying the microstructure[11,16,17] that the defects such as stacking faults and dislocations were present in these polycrystalline (>1 μm) SiC materials (nano-indentation hardness less than 36 GPa). However, the amount of defects were lower compared with the low temperature (i.e. 1300 °C vs 1500 °C) FBCVD SiC.[5] The discrepancies in the microstructure and mechanical properties still demand further explanation on the deformation mechanism of low temperature FBCVD SiC.

In this fundamental study on the mechanical properties of SiC, we have investigated the Young's modulus and hardness of three sub-micrometer FBCVD SiC coatings using indentation method. The microstructure and mechanical properties are explained on the basis of defects observed with a transmission electron microscope (TEM). The deformation behaviour underneath a nano-indentation is discussed.

2. Experimental details

Silicon carbide coatings were produced on top of highly dense pyrolytic carbon coatings as described in Ref. [5]. A planar view of the particle cross-section (defining the directions used in the later part of this paper) is shown in Fig. 1(a). Table 1 shows the deposition conditions of the low temperature FBCVD coatings. Densities were measured by the Archimedes method in ethanol. Composition was measured by Raman spectroscopy (Renishaw 1000 Raman system with a 514 nm argon laser source), with a single spot measurements of around 1 μm diameter through an 50× objective lens, as shown in Fig. 1(b). Two peaks at around 794 and 970 cm^{-1} are for SiC, and the asymmetric peaks around 200–500 cm^{-1} and 1500 cm^{-1} are acoustic SiC and second order SiC, respectively (S1 coating).[5] Carbon peaks are around 1360 and 1600 cm^{-1} (S2 coating), and the peak at 520 cm^{-1} represents silicon (S3 coating).[5] It was estimated that the excess C amount is less than 1 at.% in S2 by measuring the intensity ratios of I_{1600}/I_{794} and compared to previous study,[18] where Raman spectroscopy and elemental analysis (EPMA, AES and XPS) were used. Due to lack of the Si reference, its amount was estimated to be less than 1 at.%, because no Si related peak was found by XRD which has the resolution of 0.5 at % of crystal Si.[5] Further details on FBCVD and samples are described in Ref. [5].

SiC coated fuel particles were hot mounted in copper-loaded conductive resin. To reduce influence of the surface roughness, the FBCVD SiC coatings were first ground down to obtain a flat surface, where the nano-indentation could be carried out. The flat surface was further polished using increasingly finer diamond suspensions until 1/4 μm, and finally polished using a 0.03 μm colloidal silica suspension. The thickness of the coating after final polishing was estimated to be around 60 μm. A final surface

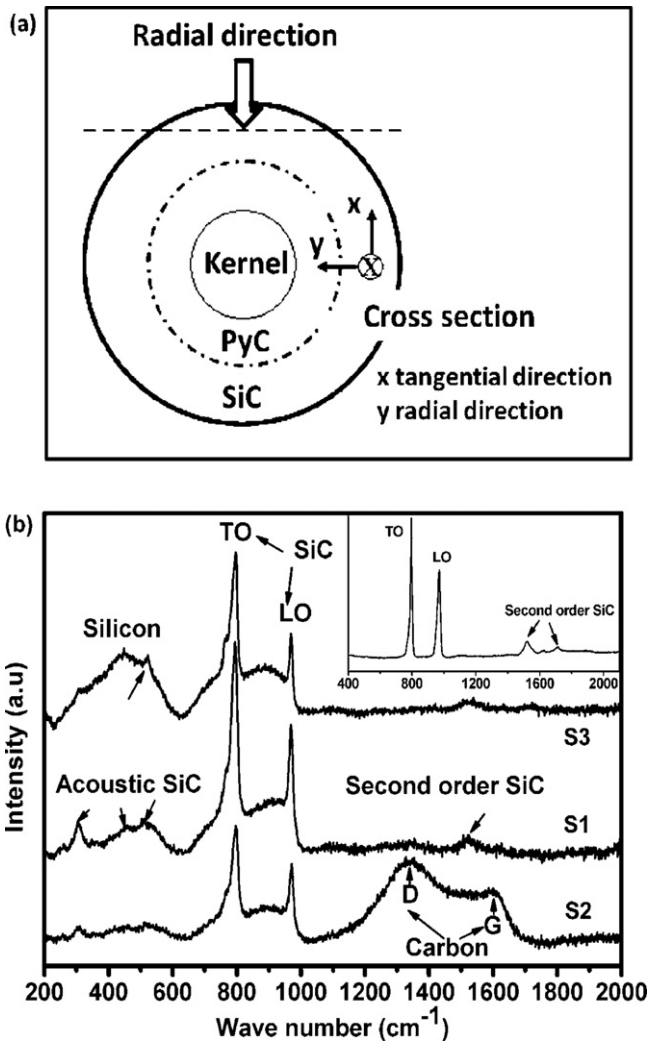

Fig. 1. (a) Schematic diagram showing a planar view of the particle cross-section: *x* and *y* are the tangential and radial directions respectively as defined in this schematic. The radial direction is always perpendicular to the particle surface. (b) Composition of nearly stoichiometric FBCVD SiC coatings detected by Raman spectroscopy, the inset is the Raman result of bulk CVD SiC (Rohm & Haas Ltd., UK).

roughness of <5 nm was detected by atomic force microscopy (AFM).

Young's modulus and hardness were measured using a nano-indenter^{TM} XP (MTS System Corp., USA) and a micro-indenter (CSM Instruments, Switzerland). Nano-indentation was made using a Berkovich indenter calibrated with a standard silica specimen. Before the measurement, the initial contact of the indenter with the specimen surface was checked, and the compliance of the loading column was corrected. Arrays of indentations were performed on each specimen with an interval of 20 times the indentation depth between each indentation. The penetration depth for the measurement of Young's modulus and hardness was 500 nm. All data were analyzed using the Oliver and Pharr method.[7] Micro-indentation was made using a Vickers indenter at a maximum load of 3 N, and the interval between each indentation was also kept to 20 times the indentation depth of ~2.6 μm. Moreover, a high purity (>99.9995%) and fully dense

Table 1
Deposition conditions of the low temperature FBCVD SiC coatings.

Codes	H_2/MTCS (vol/vol)	Additives	Temperature	Density (g/cm^3)
S1 (SiC)	10	0.1 vol% propylene	1300 °C	3.173 ± 0.029
S2 (SiC + C)	10	1.0 vol% propylene	1300 °C	3.135 ± 0.034
S3 (SiC + Si)	10	–	1300 °C	3.188 + 0.002

SiC + C or SiC + Si means that the coating is nearly stoichiometric, with low excess C or Si less than 1 at.%.

polycrystalline 3C–SiC bulk sample fabricated by static CVD (Rohm & Haas Ltd., UK) was used as a reference sample in order to confirm the accurate mechanical property measurements for FBCVD SiC coatings. The Raman spectroscopy of bulk CVD SiC was the inset in Fig. 1(b), and no excess C or Si was found in it.

To observe the grain morphology more clearly, the coatings were chemically etched using Murakami's solution (10 g sodium hydroxide and 10 g potassium ferricyanide in 100 ml of boiling water). The surface morphology of coatings was characterised using scanning electron microscopy (Field emission gun Philips XL30 FEG-SEM).

A transmission electron microscope, TEM (FEG-TEM: Tecnai^{TM} G^2 F30 U-TWIN, 300 kV) was used to study the microstructure of the coating layer before and after indentation. For cross-sectional analysis, TEM samples were prepared using a focused ion beam (FIB, FEI Nova 600 Dual Beam system) milling. For high resolution TEM (HRTEM), the samples were prepared using an ion beam milling method.

3. Results

3.1. Hardness and Young's modulus

Fig. 2 shows the hardness (H) and Young's modulus (E) as a function of composition of the three types of coatings. Measurements were made in the radial direction of SiC coatings and static bulk CVD SiC for both micro- and nano-indentation, to give reliable comparison with previous studies.[19–22] As the reference material, the nano-hardness (36 GPa) and Young's modulus (496 GPa) of bulk CVD SiC are nearly the same as previous study[19] which are 36 GPa and 503 GPa, respectively. From Fig. 2(a), it can be seen that S1 has a higher hardness compared with S2 and S3. Further, it was found that the values of hardness obtained by nano-indentation (Fig. 2(a)) were higher than by micro-indentation for all samples. For the low temperature FBCVD coatings, the nano-hardness is observed to vary in the range 39 GPa to 44 GPa while the micro-hardness varies between 36 and 42 GPa. These values are at least 8% higher than the bulk static CVD SiC which has a nano-hardness ~36 GPa and a micro-hardness ~32 GPa (see Fig. 2(a)). Moreover, it was seen that the low temperature FBCVD SiC coatings have higher hardness as compared to a previous study of CVD SiC, for which the hardness values varied in the range of 25–39 GPa as measured by nano-indentation under the similar experimental conditions.[19–22] For the FBCVD SiC coatings, Young's modulus of all three coatings was lower than the bulk CVD SiC (see Fig. 2(b)). However, this is around the value of 438 GPa, which is an average Young's modulus value of polycrystalline CVD SiC reported by Roy et al.[23] (see Table 1 in Ref. [23]). It should be noted that the difference in hardness and Young's modulus data could not be simply explained by the existence of C or Si, due to their low concentration (<1 at.%) and location in the coatings, which has been addressed in detail in previous study.[24] This indicates that the difference of hardness and modulus could be related to other microstructure, such as pores which could vary from atomic scale to micrometres, which is discussed in the following session.

Both nano- and micro-hardness results (Fig. 2(a)) are higher than the available data for polycrystalline CVD SiC[19–22] as discussed above, and the correct measurement of SiC coatings with

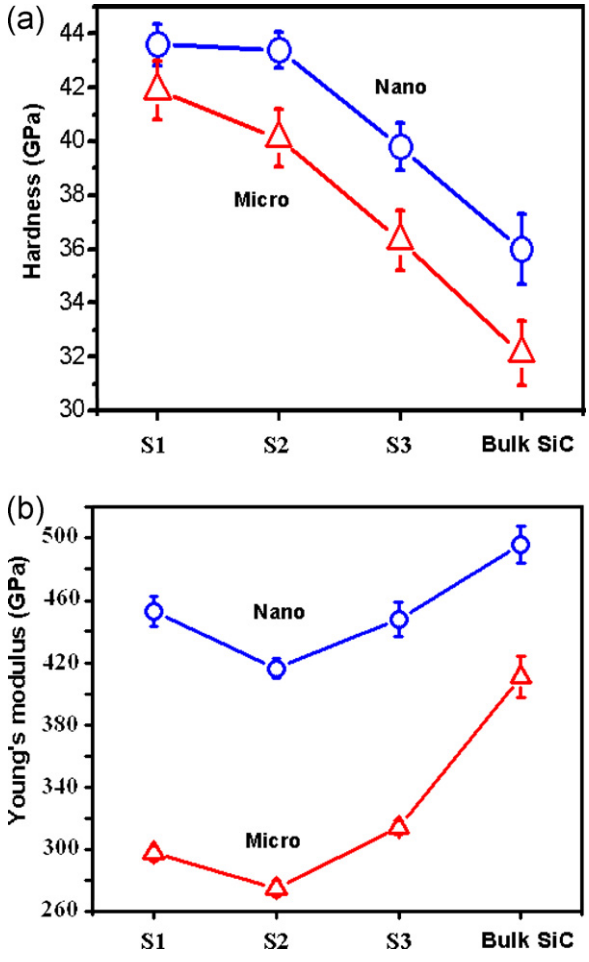

Fig. 2. Mechanical properties of three types of coating samples and bulk CVD SiC (Rohm & Haas Ltd., UK), (a) the hardness (b) Young's modulus.

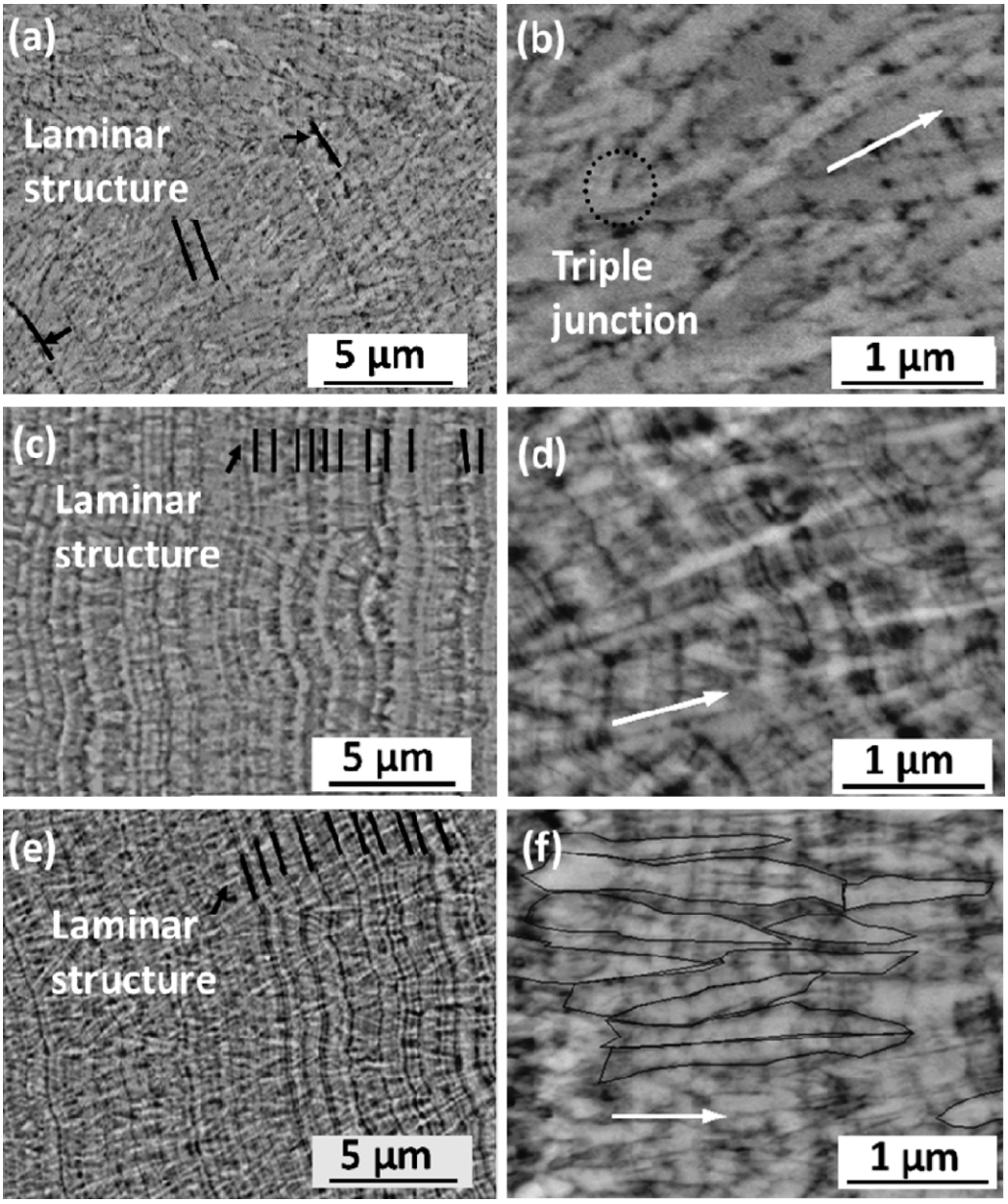

Fig. 3. SEM images showing the microstructure for (a) and (b) etched S1 (SiC) coating, (c) and (d) etched S2 (SiC + C) SiC coating, (e) and (f) etched S3 (SiC + Si) SiC coating. White arrows indicate the coating growth direction.

small dimensions was ensured by comparing with the bulk CVD SiC. As mentioned, the hardness and Young's modulus measured by micro-indentation are slightly lower than the values measured by nano-indentation, because cracks were formed under micro-indentation due to the higher indentation load.

3.2. Microstructure of low temperature FBCVD SiC

Fig. 3 shows SEM images of the three etched FBCVD SiC coatings. In all three coatings, the width and length of columnar grains were found to be approximately 200 nm and 1–2 μm respectively. These are found to be much smaller than the SiC coating produced at a temperature of 1500 °C which had width ~1 μm and length ~4–5 μm.[17] They are also smaller than the SiC showing dislocation movement under the indentation deformation zone, which was produced at temperature of 1500–1600 °C by FBCVD and 1500 °C by static CVD with grain size of 1–5 μm and 5–10 μm respectively.[11,16]

Although the grain size is in the similar range for three coatings (as mentioned above), due to different deposition conditions, the grain morphologies of three coatings vary significantly. First, a less laminar structure was observed in the S1 coating (see Fig. 3(a)) as compared to the coatings with excess C or Si (Fig. 3(c) and (e)). Fig. 3(b) shows the existence of triple junctions that could resist the movement of grain boundaries and dislocation slip.[12] Pores were also observed along the laminar structure after etching. In the S2 coating, it has a large amount of a laminar structure running through a single grain as illustrated in Fig. 3(d). The information of grain morphology in S2 was covered by the laminar structure perpendicular to the growth

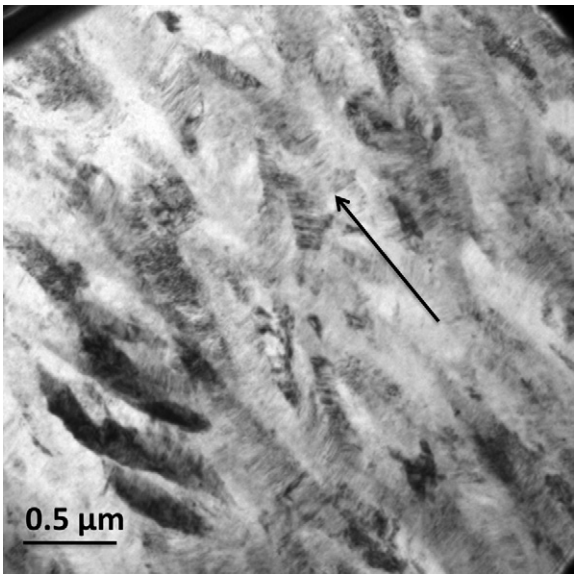

Fig. 4. Bright field TEM image of the S2 (SiC + C) coating shows the grain interaction with each other, and the arrow indicates grain growth direction.

direction after etching (Fig. 3(d)). To get more information about the grains morphology in S2 coating, the TEM image was taken and given in Fig. 4. Fig. 4 shows that grains in S2 coating interact with each other, which is similar as in sample S1 (Fig. 3(b)), and grains form branch like structures. In the S3 coating (as can be seen in Fig. 3(f)), a parallel growth of grains with less interaction among grains was observed.

According to previous study[24] about the grain boundary morphology, it was found that the grain boundary in S3 coating is smooth, while in S1 and S2 coating the grain boundaries are rough.[24] It could be attributed to the different C/Si ratio in reaction gas, and it could produce the SiC with different morphologies on (1 1 1) crystal plane, which may have three different morphologies, rough, smooth and pyramidal defect.[25] Grains with differently finished surfaces could lead to different grain growth morphologies because of different surface energy. For example, in rough grain boundaries of S1 and S2 coatings, branch like crystals were found, as in Figs. 3(b) and 4.

Fig. 5 shows bright field TEM images of the S1 coating, S2 and S3 coatings. The columnar grains were observed to grow perpendicular to the coating surface which was consistent with the SEM results. Further, nano porous layers normal to the coating growth direction were observed in the S2 coating (see Fig. 5(b)). The formation of porosity in thin films could be attributed to differences in diffusion of growth species, the incident molecule direction and deposition of secondary phases such as excess Si or C.[26] At low deposition temperatures the probability of a precursor reaching the edge of the nucleus is considerably lower compared that of arriving on the top due to a low surface diffusion. As these nuclei grow, the areas immediately around them will suffer from a shadowing effect, blocking the arrival of new molecules and the formation of new nuclei. Since the diffusivity of atoms is low and no new nuclei are formed in those regions, gaps will be formed among grains. A wrinkled like defect layer was seen in the S3 coating (Fig. 5(c)), which could be attributed to the interruption of the SiC crystallization growth during the deposition process, such as crystal lattice misorientation, as seen in Fig. 6. No obvious laminar defect was observed in the S1 coating by TEM, this could be due to the less interruption during deposition process. According to above observation, it was proposed that the laminar structure observed in SEM images indicates some instability during fabrication process, resulting in the deposition of the nano- and micro-pores and misorientation. This was attributed the variations in circulation and deposition occurred close to the nozzle or at the hot zone.[5]

Stacking faults were observed for all three types of samples as shown in Fig. 5 with a higher density than for the SiC deposited at a temperature of 1500 °C.[11,16,17] These stacking faults could cause an intrinsic residual stress due to the coexistence of the partial dislocations. This was supported by the high resolution TEM images (shown in Fig. 7) exhibiting wave pattern fringes, and they could only be observed in one direction which is determined by the intrinsic stress.

Since the dislocation mobility under nano-indentation deformation has not been fully understood in hard ceramic materials, therefore, it is significant to study this behaviour in FBCVD SiC coatings with a sub-micrometer grain size. However, it is difficult to observe the dislocations under the two-beam or weak beam dark field conditions due to the high density of defects. In the present study, the reversed fast Fourier transform (FFT) images of the corresponding high resolution TEM images was used to obtain information about the dislocations. This method has been used in many cases for dislocation observations.[27]

Fig. 8(a) shows a high resolution TEM image of a S1 coating which was taken as a representative image to compare the atomic structure of all three coatings. Fig. 8(b) is the reverse FFT image using the marked inset diffraction pattern of Fig. 7(a), in which sessile and glide dislocations can be observed. The dislocation density was calculated from the total number of glide dislocations divided by the area in single image.[28,29] From the analysis of images shown in Fig. 8, the dislocation density in S1 coatings was found to be $10^{13}/cm^2$. The same magnitude of dislocations density was found in the S2 and S3 coatings, as shown in Fig. 7 (three HRTEM images were analyzed for each coating).

3.3. Deformation behaviour under the indentation

The deformation zone under the indentation was investigated through the images of FIB milled TEM samples in order to study the deformation mechanism of the low temperature FBCVD SiC coatings. Fig. 9 shows the bright field TEM images showing the mechanical behaviour of a S1 coating under nano-indentation in the radial direction at a maximum indentation depth of 500 nm.

Fig. 9(a) is an overview of the deformation area under an indentation. A median crack has formed just underneath the surface and has a direction aligned with the indenter tip impression. A higher magnification image around the elastic and plastic interface is shown in Fig. 9(b). It can be seen that a large amount of inter-granular and trans-granular micro cracks

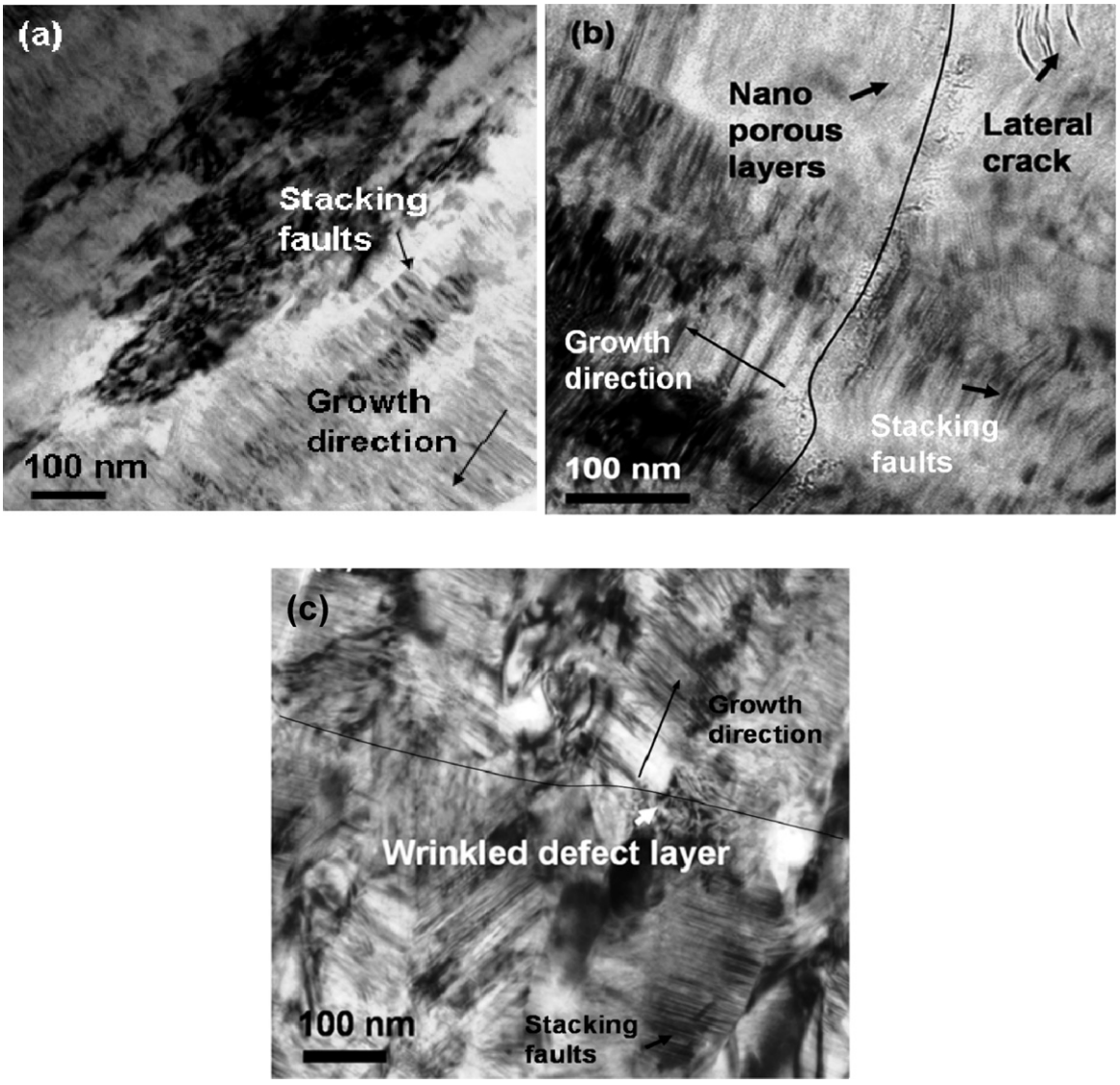

Fig. 5. Bright field TEM images of three SiC based coatings; (a) the S1 (SiC) with stacking faults perpendicular to the growth direction (b) the S2 (SiC + C) showing the laminar nanoporous layer (c) the S2 (SiC + Si) with a wrinkled like defects layer.

were produced around the median crack initiation zone. This is substantially different from the dislocation-related plastic deformation behaviour,[10,11,16,30] which usually has a severe plastically deformed region with few or no cracks. Moreover, the micro cracks were also observed in the C and D zones under the indentation. Fig. 9(c) shows that micro cracks that are formed along the grain boundaries which are tending to follow the shear band direction with the formation of a few trans-granular cracks. In Fig. 9(d), it can be seen that shear band micro cracks were formed in one single grain (see inset in the left bottom corner of Fig. 9(d)). This single grain has a large amount of defects which are supposed to be the as-deposited defects as shown in Fig. 5(a). Shear band cracks were also observed just underneath the indenter tip (right top inset in Fig. 9(d)). As a result, a shear band dominated deformation zone can be seen in Fig. 9(c and d) under the indentation in a S1 coating.

The S2 and S3 coatings only show a micro crack pattern which is different from S1 coating. Fig. 10 gives the TEM images of the S2 and S3 coatings showing the mechanical reaction underneath the indentation. It can be seen from Fig. 10(a) and (c) that the median cracks are not always produced under the indentation for S2 and S3 coatings. However, some irregular cracks in S3 coatings and lateral cracks in S2 were produced. In particular, in the S3 coating (Fig. 10(b)), more micro cracks either intragrain or transgrain were found than in the S1 and S2 coatings. This is due to the fact that the most micro cracks propagate along the grain boundaries in S1 and S2 coatings (Figs. 9(b) and 10(d)). A careful analysis of the TEM images shows that only micro cracks were found under the indentation and no dislocation-induced shear band was observed. This is different from previous studies on the deformation behaviour of polycrystalline SiC.[11,16,30] For example in bulk polycrystalline CVD SiC,[11] it was found that it has more dislocation slip bond rather than micro cracks either in grains or along grain boundaries, even though the indentation load is higher than the load used in the FBCVD SiC based materials. The possible

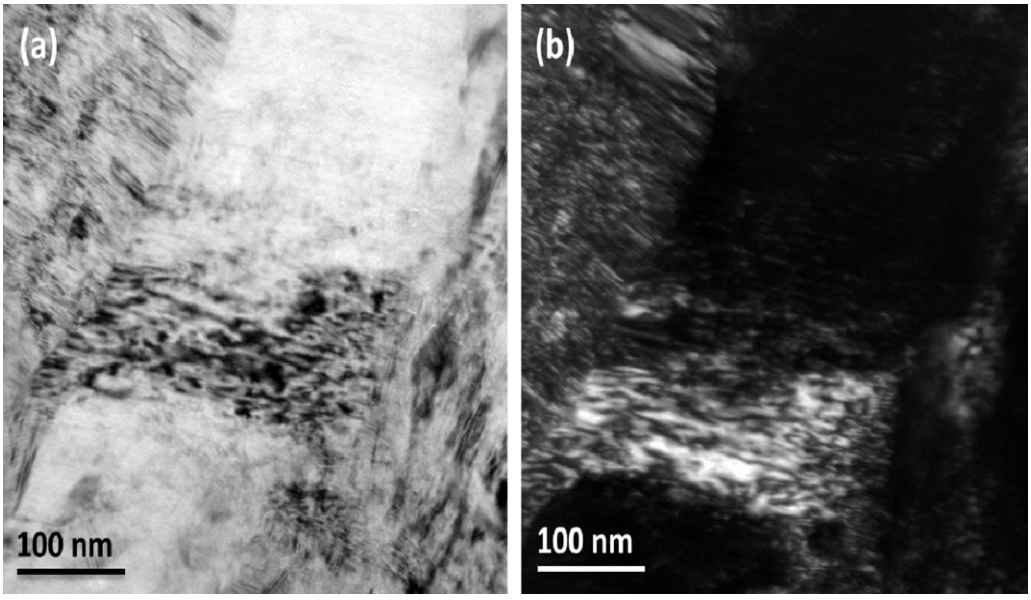

Fig. 6. An example of the crystal misorientation formed during SiC deposition, (a) BF-TEM and (b) DF-TEM.

reason of this discrepancy is discussed later. Moreover, no amorphous phase and α-SiC phase was formed under the indentation observed by diffraction and bright field TEM images, which is consistent with the work of Mishra and Szlufarska.[31]

4. Discussion

As described above, high hardness and Young's modulus were obtained in the sub-micrometer grain size coatings produced at a low temperature by FBCVD. In the S1 coatings, the nano-hardness is ∼22% higher while the micro-hardness is ∼31% higher compared to a commercial CVD SiC. The higher hardness was also obtained in S2 and S3 coatings. All the coatings retained a higher Young's modulus than those SiC materials having high hardness in previous study (equal or higher than 40 GPa nano-hardness),[32] making these coatings unique among polycrystalline phase brittle ceramic material.

As mentioned above (Section 3), under the nano-indentation only micro cracks were found in the deformation zone. Our results seem to be consistent with the conventional view of the failure mechanism of brittle ceramics at room temperature[33]: the lack of dislocation and the high Peierls force are reasons for fracture to occur in brittle materials. However, dislocation-related plastic deformation routinely occurred in hardness testing, because the indentation stress field offers conditions of stress conductive to plastic deformation.[11,13,16,33] Molecular dynamic simulations even demonstrate that 1/3 of the hardness-related deformation is from dislocation-related plastic deformation, while 2/3 comes from fracture in SiC.[30] It is rare to see a deformation zone dominated by micro cracks in polycrystalline SiC, such as in FBCVD SiC coatings (Figs. 9 and 10, and see for example Refs. [11,16,30]). With the above questions, we first estimated the factors controlling Young's modulus in FBCVD SiC coatings followed by a study of mechanism of superior hardness and deformation under an indentation, which influence the hardness in the three coatings.

4.1. Influence of porosity on Young's modulus

Young's modulus presents a material constant for uniaxial tensile deformation, which is physically related to the atomic spacing, inter atomic bond strength and bond density. In a previous study[5] on a low temperature FBCVD SiC coating, it was shown from XRD measurements that a shoulder peak was observed in addition to the β-SiC (1 1 1) diffraction peak, which corresponded to a crystal plane spacing of ∼0.266 nm. Moreover, through the observation of their results, we found that the XRD peak shifted to a lower diffraction angle. According to the XRD pattern (Fig. 11 in Ref. [5]), the crystal lattice constants of ∼0.4366, 0.4368 and 0.4368 nm for S1, S2 and S3 coatings were obtained, respectively, while the crystal lattice constant for bulk CVD SiC is ∼0.4359 nm (XRD pattern obtained by the same condition was shown in Ref. [24]). Further, crystal orientation, impurities and porosity may affect the Young's modulus. As the Young's modulus in the radial direction was similar to the value obtained along the cross-section[5,24] which meant that the orientation has no effect on Young's modulus. Moreover, as discussed before the effect of C or Si in S2 was found to have no effect on the difference of hardness and Young's modulus. Excluding these two factors (orientation and impurities); the effect of porosity on variation of the elastic properties in three coatings was investigated. The presence of nano-pores in S2 coating as in Fig. 5(b) results in a lower density. Although no pores were directly observed by TEM in the S1 and S3 coatings, their density is lower than the theoretical density of SiC. Thus, the elastic modulus E at room temperature can be expressed in an exponential function of porosity V_p[34] as:

$$E = E_0 \exp(-CV_p), \quad (1)$$

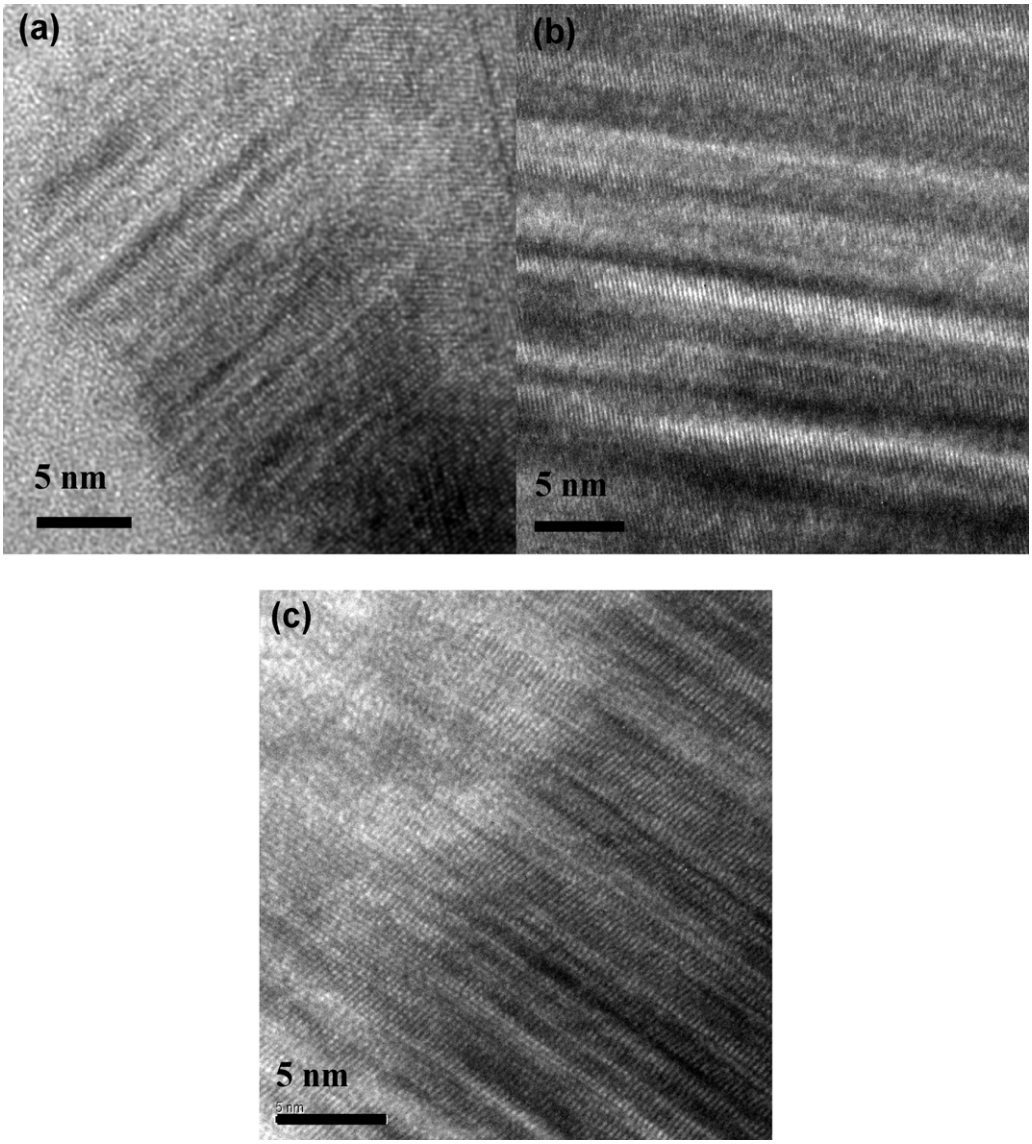

Fig. 7. High resolution TEM images for three FBCVD SiC coatings; (a) S1 (SiC) (b) S2 (SiC + C) and (c) S3 (SiC + Si).

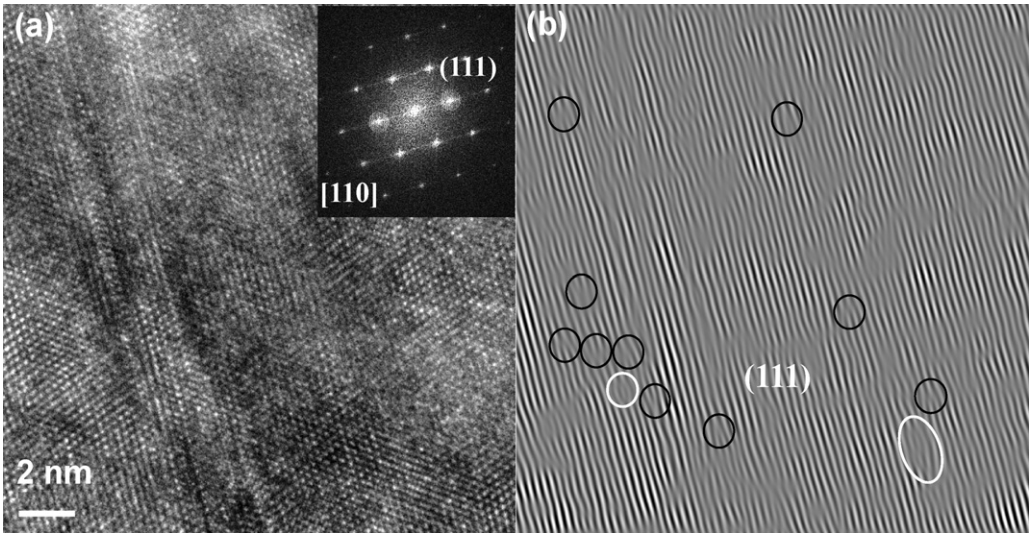

Fig. 8. TEM Images showing the defects in S1 (SiC) coating (a) (1 1 0) plane; (b) reverse FFT image, the black circles are glide dislocations and the white circles are sessile dislocations.

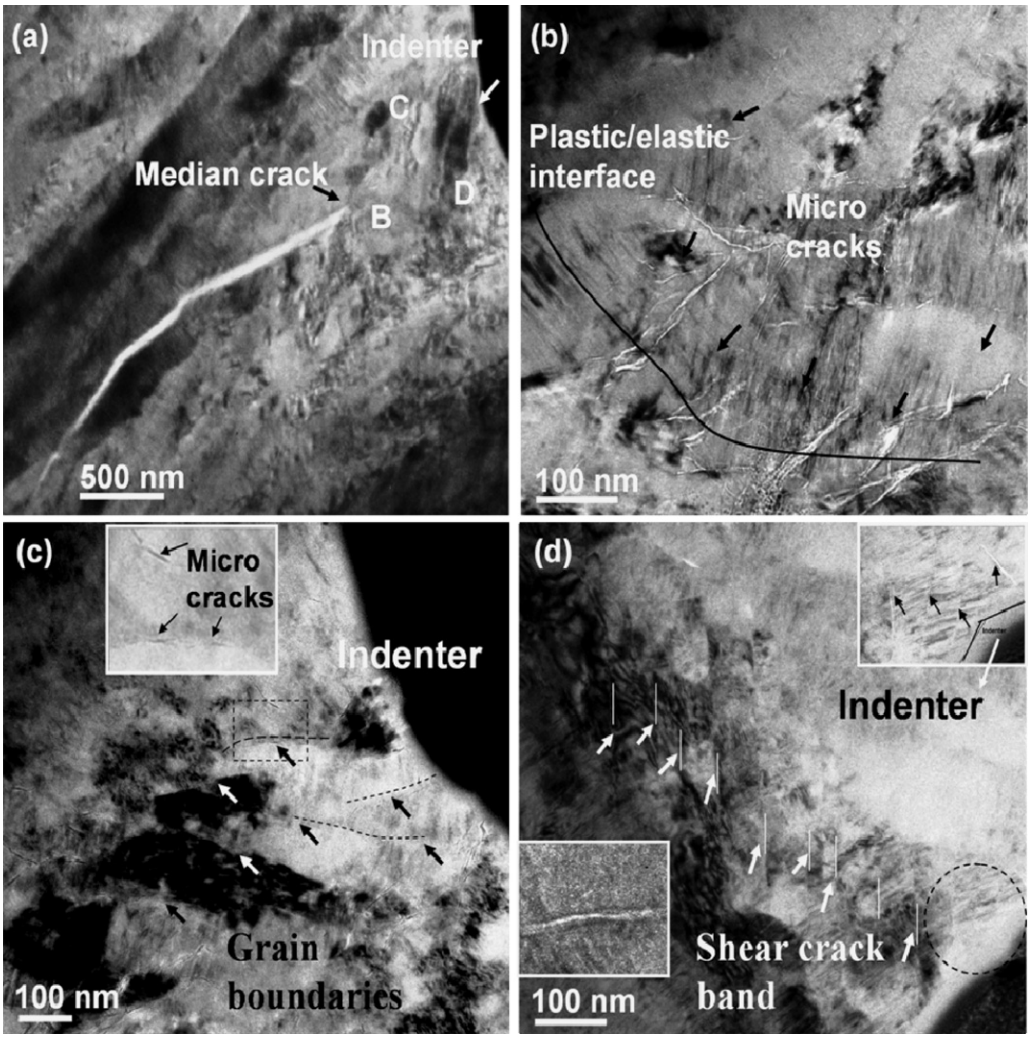

Fig. 9. Bright field TEM images of the deformed zone under a nano-indentation of a S1 (SiC) coating; (a) an overview of the deformation zone; higher magnification images of the zone marked as B, C, D in Fig. 7(a) are shown in (b), (c) and (d) respectively. Inset in (c) shows the micro cracks in the dashed square. Left bottom inset in (d) shows a high magnification of a shear crack while right upper inset in (d) shows a high magnification of the dashed circle under the indenter tip.

where $E_0 = 496$ GPa is the elastic modulus and $C = 3.57$ is a constant for a pore-free bulk CVD SiC. V_p is the ratio of the relative density difference to the theoretical density of SiC (3.22 g/cm^3).

The calculated Young's modulus for S1, S2 and S3 coatings is 465 ± 15, 446 ± 17 and 473 ± 1 GPa, respectively, which follows a trend similar to the experimental data presented in Fig. 2. It was concluded that the different Young's modulus in the three low temperature FBCVD SiC coatings is attributed to the porosity, although the experimental Young's modulus data of FBCVD SiC coatings is slightly lower than the values calculated using equation. The difference between calculated and measured value of FBCVD SiC coatings is due to that the E_0 from pore-free bulk CVD SiC instead of pore-free FBCVD SiC coatings (not available). FBCVD SiC coatings have larger crystal lattice constant (~0.437 nm) than bulk CVD SiC (~0.4359 nm) as discussed above. Since the expanded lattice constant leads to the decrease of the Young's modulus according to previous study,[19] the E_0 of pore-free FBCVD SiC coating is expected to be lower than bulk CVD SiC.

4.2. Mechanism for high hardness

From previous studies,[10,11,16,30] it is known that dislocation nucleation and glide is the primary response of SiC under nano-indentation. Formation of shear bands due to dislocations has also been reported,[11] which were found under the plastic deformation zone when indentations were made on a particular grain in polycrystalline SiC and at the grain boundaries. Moreover, it is also known from Ref. [31] that dislocation nucleation is correlated with the discrete pop-ins observed in the load-displacement curve. In the present study, no pop-ins was found due to the presence of a large amount of dislocations. Thus, dislocation mobility can be estimated similar to the case of a metallic material having intrinsic dislocations. Mishra and Szlufarska[31] worked on the dislocation mobility in 3C–SiC using large-scale molecular dynamics simulations. The results indicated that dislocation mobility decreased by dislocation interaction as its density reached a saturation value. This is similar to the work hardening effect in a metallic material.[33] We estimated the

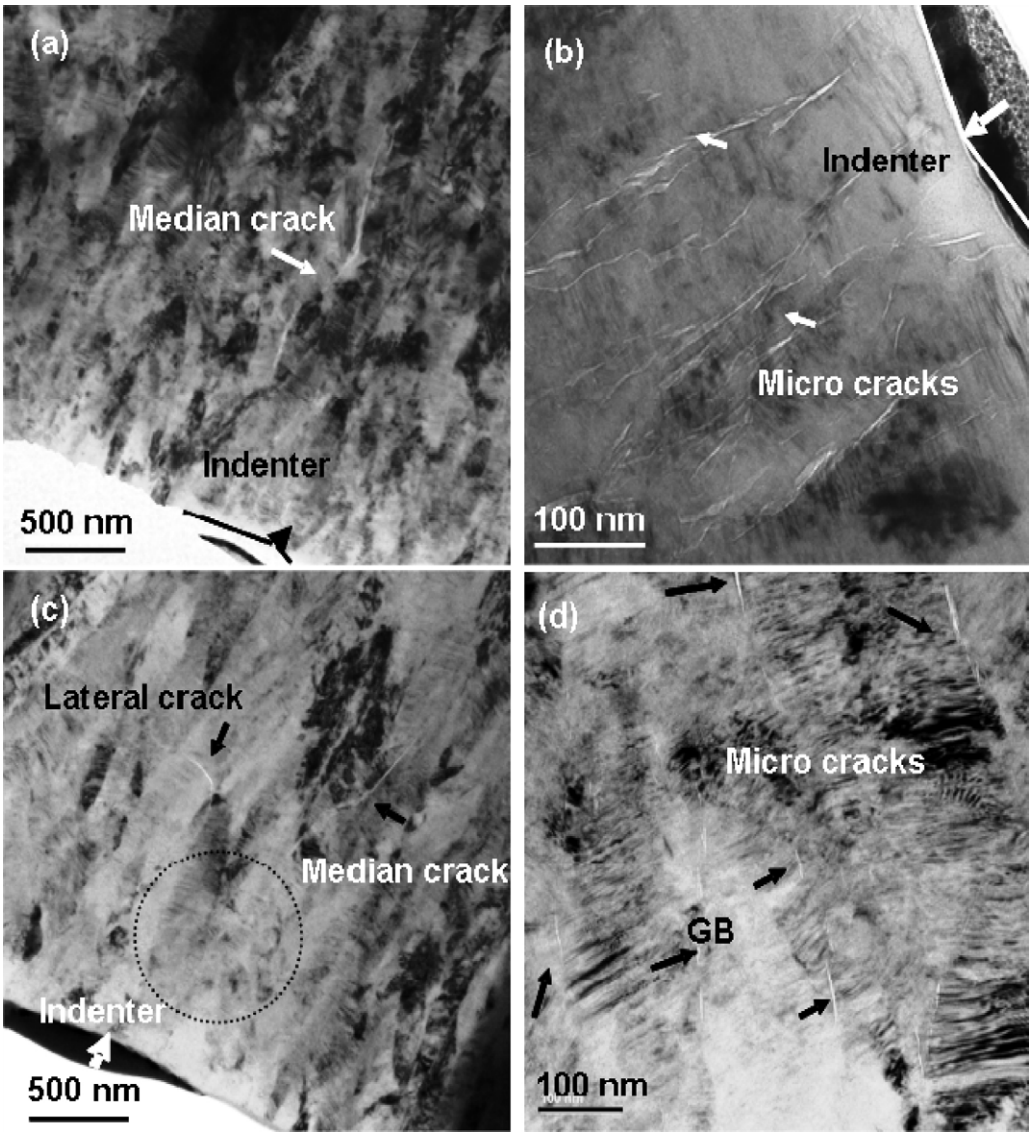

Fig. 10. TEM bright field images show the mechanical reaction underneath the indentation, (a) and (b) S3 (SiC + Si) SiC coating, (c) and (d) S2 (SiC + C) SiC coating.

dislocation mobility τ using Taylor's work hardening equation[33] given by:

$$\tau = \tau_0 + \alpha G b \rho^{1/2} \quad (2)$$

where τ_0 is the shear stress for a dislocation to move without any obstacle, and the value of τ_0 taken was 7.5 GPa[13]; α is a numerical constant depending on the locking strength of a nod. The value of α taken was 8[35]; b is Burgers vector, where $b = 0.308$ nm for a dislocation in SiC initiated and gliding on a close packed (1 1 1) plane, and ρ is the density of glide dislocations; G is the shear modulus which can be written as:

$$G = \frac{E}{2(1+\upsilon)} \quad (3)$$

where υ is the Poisson's ratio and E is the Young's modulus. The dislocation density was $\sim 0.3 \times 10^{12}/\text{cm}^2$. The calculated work hardening shear stress according to Eq. (2) was ~90 GPa. This value of the work hardening shear stress is much higher than the critical shear stress needed for the dislocation nucleation and propagation in SiC crystals, for which, the theoretical shear stress is in the range of 29.5–43.12 GPa obtained from previous reports.[36–38] Thus, the dislocation-related yield behaviour could not occur under the plastic deformation zone in sub-micrometer FBCVD SiC coatings.

As the hardness is proportional to the yield stress[33] therefore, the superior hardness value in FBCVD SiC coatings is attributed to the immobility of the dislocations. In the case of the SiC–C solid solution,[39] the occurrence of a high density of dislocations causes a strain-hardening effect. Furthermore, given that dislocations could be motivated by the shear stress, a phase transformation from a crystalline phase to an amorphous could occur.[31] However, no amorphous phase was observed under the nano-indentation (Figs. 7 and 8), nor was dislocation movement band observed in this study. This suggests that the dislocation-related phase transformation did not occur under the indentation.

4.3. Deformation mechanism under nano-indentation

The hardness-related plastic deformation, which occurs due to the nucleation and propagation of micro cracks in FBCVD SiC coatings, can be explained as follows;

(i) The onset of plastic deformation under the indentation occurs as the maximum shear stress approaches the yield stress.[40] According to $H = 1.5Y$ (Y is the yield stress; H is the hardness), the yield stress in FBCVD SiC coatings is around 26 GPa. This yield stress is lower than the stress needed for the movement of dislocations and the theoretical shear stress.[36–38] This indicates that the hardness-related plastic deformation first occurred by the nucleation of defect-induced cracks, which propagated to the indented surface (see inset (top right) in Fig. 9(d)). The deformation impression was accommodated by the densification of defects, such as the pores, dislocation pile ups and grain boundaries as in Fig. 3(b).

(ii) The shear stress was used to promote the movement of dislocations under the indentation and form slip bands in previous studies.[10,11,41] However, the highest amount of micro cracks were observed in FBCVD SiC coatings, contrary to plastic deformation under the indentation found in previous studies.[10,11,41] The micro cracks formed in the hardness-related plastic deformation zone is the Mode-II crack,[42] as shown in Fig. 9(c) and (d). Unlike Mode-I which is dominated by the tensile stress, a Mode-II crack is the consequence of a confined shear stress.[33] At the interface of the elastic/plastic deformation, branch-like micro cracks were observed, as in Fig. 9(b). All these phenomenon distinguish the hardness-related plastic deformation mechanism in FBCVD from previous studies on ceramics, which showed dislocations are the main deformation mechanism underneath the indentation.[30,43]

As described above, a unique hardness-related plastic deformation mechanism was used to explain the difference in hardness of all three types of FBCVD SiC coatings. According to Qian et al.,[44] the hardness could reach an asymptotic value with the saturation of the micro cracks growth population. In three FBCVD SiC coatings studied here, different amounts of micro cracks were found (Figs. 9(b) and 10(b and d)) and micro cracks nucleated at stress concentration zones, such as the grain boundaries or defects within the grains. Thus the difference in hardness was attributed to the grain morphologies, as shown in Fig. 3, which gives different degree of resistance to the initiation and propagation of micro cracks. In the S1 coating, triple junctions hamper grain boundary shear by forming interlocks[12] which could resist and deflect the initiation and propagation of micro cracks. In the S2 coating, elongated grains interact with the surrounding small grains which could also provide interlocks (Figs. 3(d) and 4). The slightly lower hardness of the S2 coating as compared to the S1 coating is due to the nano pores, as seen in Fig. 5(b). A lack of triple junctions and grain interactions could be the reason for the lower hardness in the S3 coating, as it has a parallel crystalline morphology which has less constraint towards the initiation and propagation of cracks.

5. Conclusions

The microstructure and mechanical properties of three types of FBCVD SiC coatings (SiC, SiC + C and SiC + Si) were studied. FBCVD SiC coatings with a sub-micrometer grain size were deposited on simulated TRISO fuel particles by FBCVD at a low temperature (1300 °C). The mechanical properties were studied using micro and nano-indention. The microstructures were studied using SEM and TEM. It was found that the Young's modulus of all three coatings differ which was attributed due to the presence of nano-pores. The high hardness of FBCVD SiC coatings was due to the large amount of defects, particularly the high density of dislocations. It is found that the interactions between dislocations reduced their mobility and make dislocation-related plastic deformation unavailable. We suggest that the work hardening effect is the reason for the high hardness in the sub-micrometer grain size FBCVD SiC coatings. A hardness related-deformation mechanism was attributed to the initiation and propagation of micro cracks. The nano-indentation indent volume is most likely be accommodated by the densification of defects such as the pores. As a result, the hardness difference in FBCVD SiC coatings is due to the different grain morphologies producing different amounts of micro cracks.

Acknowledgements

The authors would like to acknowledge the English support provided by Professor Brain Ralph.

References

1. Snead LL, Nozawa T, Katoh Y, Byun TS, Kondo S, Petti DA. Handbook of SiC properties for fuel performance modeling. *J Nucl Mater* 2007;**371**:329–77.
2. Miller GK, Petti DA, Varacalle DJ, Maki JT. Statistical approach and benchmarking for modeling of multi-dimensional behavior in TRISO-coated fuel particles. *J Nucl Mater* 2003;**317**:69–82.
3. Petti DA, Buongiorno J, Maki JT, Hobbins RR, Miller GK. Key differences in the fabrication, irradiation and high temperature accident testing of US and German TRISO-coated particle fuel, and their implications on fuel performance. *Nucl Eng Des* 2003;**222**:281–97.
4. Kadak AC, Gnallinger R, Driscoll MJ, Yip S, Wilson DG, No HC, et al. Modular pebble bed reactor. In: *Modular pebble bed reactor project University research consortium annual report*. 2000.
5. Lopez-Honorato E, Meadows PJ, Tan J, Xiao P. Control of stoichiometry, microstructure, and mechanical properties in SiC coatings produced by fluidized bed chemical vapor deposition. *J Mater Res* 2008;**23**:1785–96.
6. Tan J, Meadows PJ, Zhang D, Chen X, Lopez-Honorato E, Zhao X, et al. Young's modulus measurements of SiC coatings on spherical particles by using nanoindentation. *J Nucl Mater* 2009;**393**:22–9.
7. Oliver WC, Pharr GM. An improved technique for determining hardness and elastic-modulus using load and displacement sensing indentation experiments. *J Mater Res* 1992;**7**:1564–83.
8. Chien CH, Jian SR, Wang CT, Juang JY, Huang JC, Lai YS. Cross-sectional transmission electron microscopy observations on the Berkovich indentation-induced deformation microstructures in GaN thin films. *J Phys D: Appl Phys* 2007;**40**:3985–90.

9. Tan JC, Merrill CA, Orton JB, Cheetham AK. Anisotropic mechanical properties of polymorphic hybrid inorganic–organic framework materials with different dimensionalities. *Acta Mater* 2009;**57**:3481–96.
10. Page TF, Rester L, Hainsworth SV. The plasticity response of 6H-SiC and related isostructural materials to nanoindentation: slip vs densification. *Mater Res Soc Symp Proc* 1998;**522**:113–8.
11. Zhao X, Langford RM, Shapiro IP, Xiao P. Onset plastic deformation and cracking behaviour of 3C—SiC upon indentation at room temperature. *J Amer Ceram Soc* 2011;**94**:3509–14.
12. Grabco D, Shikimaka O, Harea E. Translation-rotation plasticity as basic mechanism of plastic deformation in macro-, micro- and nanoindentation processes. *J Phys D: Appl Phys* 2008;**41**:074016–74024.
13. Chen HP, Kalia RK, Nakano A, Vashishta P, Szlufarska I. Multimillion-atom nanoindentation simulation of crystalline silicon carbide: orientation dependence and anisotropic pileup. *J Appl Phys* 2007;**102**: 063514–63522.
14. Szlufarska I, Kalia RK, Nakano A, Vashishta P. Atomistic mechanisms of amorphization during nanoindentation of SiC: a molecular dynamics study. *Phys Rev B* 2005;**71**:174113–23.
15. Szlufarska I, Nakano A, Vashishta P. A crossover in the mechanical response of nanocrystalline ceramics. *Science* 2005;**309**:911–4.
16. Chollon G, Vallerot JM, Helary D, Jouannigot S. Structural and textural changes of CVD-SiC to indentation, high temperature creep and irradiation. *J Eur Ceram Soc* 2007;**27**:1503–11.
17. Hélary D, Bourrat X, Dugne O, Maveyraud G, Pérez M, Guillermier P. Microstructures of silicon carbide and pyrocarbon coatings for fuel particles for high temperature reactors. In: *2nd international topical meeting on high temperature reactor technology*. 2004.
18. Dong SM, Chollon G, Labrugere C, Lahaye M, Guette A, Bruneel JL, et al. Characterization of nearly stoichiometric SiC ceramic fibres. *J Mater Sci* 2001;**36**:2371–81.
19. Osborne MC, Hay JC, Snead LL, Steiner D. Mechanical- and physical-property changes of neutron-irradiated chemical-vapor-deposited silicon carbide. *J Am Ceram Soc* 1999;**82**:2490–6.
20. Park KH, Kondo S, Katoh Y, Kohyama A. Mechanical properties of beta-SiC after Si- and dual Si plus He-ion irradiation at various temperatures. *Fusion Sci Technol* 2003;**44**:455–9.
21. Nagappa S, Zupan M, Zorman CA. Mechanical characterization of chemical-vapor-deposited polycrystalline 3C silicon carbide thin films. *Scripta Mater* 2008;**59**:995–8.
22. Bellan C, Dhers J. Evaluation of young modulus of CVD coatings by different techniques. *Thin Solid Films* 2004;**469–470**:214–20.
23. Roy S, Zorman C, Mehregany M, Deanna R, Deeb C. The mechanical properties of polycrystalline 3C—SiC films grown on polysilicon substrates by atmospheric pressure chemical-vapor deposition. *J Appl Phys* 2006;**99**:044108–44120.
24. Tan J. *Mechanical properties of SiC in TRISO fuel particle*. Thesis. University of Manchester; 2010.
25. Hernandez MJ, Ferro G, Chassagne T, Dazord J, Monteil Y. Study of surface defects on 3C—SiC films grown on Si (1 1 1) by CVD. *J Cryst Growth* 2003;**253**:95–101.
26. Machlin ES. *Materials science in microelectronics I. The relationships between thin film processing and structure*. 2nd ed. Oxford: Elsevier Science; 2005, 206-47.
27. Nakamura A, Yamamoto T, Ikuhara Y. Direct observation of basal dislocation in sapphire by HRTEM. *Acta Mater* 2002;**50**:101–8.
28. Shin HY, Kwon SK, Chang YI, Cho MJ, Park KH. Reducing dislocation density in GaN films using a cone-shaped patterned sapphire substrate. *J Cryst Growth* 2009;**311**:4167–70.
29. Callister WD. *Materials science and engineering: an introduction*. 7th ed. Australia: John Wiley & Sons Australia Limited; 2006, p 191–99.
30. Zhou SJ, Zhou XY, Zhao YS. Study of hardness and deformation of brittle materials with a density functional theory. *J Appl Phys* 2008;**104**:053508–16.
31. Mishra M, Szlufarska I. Possibility of high-pressure transformation during nanoindentation of SiC. *Acta Mater* 2009;**57**:6156–65.
32. Beaber AR, Qi LJ, Hafiz J, Mcmurry PH, Heberlein JVR, Gerberich WW, et al. Nanostructured SiC by chemical vapor deposition and nanoparticle impaction. *Surf Coat Technol* 2007;**202**:871–5.
33. Green DJ. *An introduction to the mechanical properties of ceramics. Cambridge solid state science series*. 1st ed. Cambridge: The University Press; 1998. p. 162–91.
34. Rice RW. *Mechanical properties of ceramics and composites*. 1st ed. New York: Marcel Dekker; 2000. p. 457–534.
35. Messerschmidt U. *Dislocation dynamics during plastic deformation, part 2, ceramic single crystals*. Springer Series in Materials Science; 2010. p. 264.
36. Ogata S, Li J, Hirosaki N, Shibutani Y, Yip S. Ideal shear strain of metals and ceramics. *Phys Rev B* 2004;**70**:104104–10.
37. Umeno Y, Kinoshita Y, Kitamura T. Ab initio DFT study of ideal shear strength of polytypes of silicon carbide. *Strength Mater* 2008;**40**:2–6.
38. Umeno Y, Cerny M. Effect of normal stress on the ideal shear strength in covalent crystals. *Phys Rev B* 2008;**77**:100101–4.
39. Mykhaylyk OO, Gadzira MP. Superhard materials based on the solid solution SiC—C. *J Mater Chem* 2001;**11**:217–22.
40. Fischer-Cripps AC. *Introduction to contact mechanics. Mechanical engineering series*. 1st ed. New York: Springer; 2000. p. 139–77.
41. Park KH, Hinoki T, Kohyama A. Influence of irradiation-induced defects on fracture behavior in highly pure SiC. *J Nucl Mater* 2007;**367**:703–7.
42. Wereszczak AA, Johanns KE, Jadaan OM. Hertzian ring crack initiation in hot-pressed silicon carbides. *J Am Ceram Soc* 2009;**92**:1788–95.
43. Lloyd SJ, Castellero A, Giuliani F, Long Y, Mclaughlin KK, Molina-Aldareguia JM, et al. Observations of nanoindents via cross-sectional transmission electron microscopy: a survey of deformation mechanisms. *Proc Roy Soc A: Math Phys* 2005;**461**:2521–43.
44. Qian J, Daemen LL, Zhao Y. Hardness and fracture toughness of moissanite. *Diam Relat Mater* 2005;**14**:1669–72.